Journal of Biomedical Optics

SPIEDigitalLibrary.org/jbo

Monitoring early tumor response to drug therapy with diffuse optical tomography

Molly L. Flexman
Fotios Vlachos
Hyun Keol Kim
Shashank R. Sirsi
Jianzhong Huang
Sonia L. Hernandez
Tessa B. Johung
Jeffrey W. Gander
Ari R. Reichstein
Brooke S. Lampl
Antai Wang
Mark A. Borden
Darrell J. Yamashiro
Jessica J. Kandel
Andreas H. Hielscher

SPIE

Monitoring early tumor response to drug therapy with diffuse optical tomography

Molly L. Flexman,[a,*] Fotios Vlachos,[a,*] Hyun Keol Kim,[a] Shashank R. Sirsi,[b,c] Jianzhong Huang,[d] Sonia L. Hernandez,[e] Tessa B. Johung,[d] Jeffrey W. Gander,[d] Ari R. Reichstein,[d] Brooke S. Lampl,[f] Antai Wang,[g] Mark A. Borden,[b,c] Darrell J. Yamashiro,[d,e,†] Jessica J. Kandel,[d,†] and Andreas H. Hielscher[a,f,h,†]

[a]Columbia University, New York, Department of Biomedical Engineering, New York, New York 10027
[b]Columbia University, New York, Department of Chemical Engineering, New York, New York 10027
[c]University of Colorado, Boulder, Department of Mechanical Engineering, Boulder, Colorado 80309
[d]Columbia University, New York, Department of Surgery, New York, New York 10032
[e]Columbia University, New York, Department of Pediatrics and Pathology, New York, New York 10032
[f]Columbia University, New York, Department of Radiology, New York, New York 10032
[g]Columbia University, New York, Department of Biostatistics, Mailman School of Public Health, New York, New York 10032
[h]Columbia University, New York, Department of Electrical Engineering, New York, New York 10027

Abstract. Although anti-angiogenic agents have shown promise as cancer therapeutics, their efficacy varies between tumor types and individual patients. Providing patient-specific metrics through rapid noninvasive imaging can help tailor drug treatment by optimizing dosages, timing of drug cycles, and duration of therapy—thereby reducing toxicity and cost and improving patient outcome. Diffuse optical tomography (DOT) is a noninvasive three-dimensional imaging modality that has been shown to capture physiologic changes in tumors through visualization of oxygenated, deoxygenated, and total hemoglobin concentrations, using non-ionizing radiation with near-infrared light. We employed a small animal model to ascertain if tumor response to bevacizumab (BV), an anti-angiogenic agent that targets vascular endothelial growth factor (VEGF), could be detected at early time points using DOT. We detected a significant decrease in total hemoglobin levels as soon as one day after BV treatment in responder xenograft tumors (SK-NEP-1), but not in SK-NEP-1 control tumors or in non-responder control or BV-treated NGP tumors. These results are confirmed by magnetic resonance imaging T2 relaxometry and lectin perfusion studies. Noninvasive DOT imaging may allow for earlier and more effective control of anti-angiogenic therapy. [DOI: 10.1117/1.JBO.17.1.016014]

Keywords: diffuse optical imaging; diffuse optical tomography; magnetic resonance imaging; angiogenesis; bevacizumab; Avastin®; therapy response; cancer imaging.

Paper 11540 received Sep. 23, 2011; revised manuscript received Nov. 25, 2011; accepted for publication Nov. 30, 2011; published online Feb. 8, 2012.

1 Introduction

The emergence of treatments that target blood vessel development in tumors has been highly effective in subsets of patients and in select types of cancer. However, the variability in efficacy, combined with the high cost and toxicity of these novel treatments, suggest that a rapid noninvasive means of benchmarking tumor response to therapy is useful. We show here the use of diffuse optical tomography (DOT) for monitoring tumor vascularization. Using two small animal xenograft model systems with previously well-characterized responses to vascular endothelial growth factor (VEGF) inhibition, we use DOT to distinguish responder from non-responder tumor types within a few days of starting treatment.

The field of anti-angiogenic research was pioneered by Judah Folkman who, 40 years ago, first suggested that the prevention of new vessel formation could result in tumor dormancy and could, therefore, be a novel cancer therapy.[1] Since that time, considerable effort has been invested in developing new anti-angiogenic agents that were tested in a number of preclinical and clinical studies. The majority of these agents target pro-angiogenic growth factors, specifically, VEGF. It has been shown that VEGF is expressed in almost all human tumors and higher levels of VEGF correlated with increased tumor vascularity, growth, invasion and metastasis.[2] The first successful human clinical trial showed that an anti-VEGF monoclonal antibody [bevacizumab (BV)] substantially increased the time of progression in metastatic colon cancer, and led to FDA approval of BV in 2004.[3,4] BV is now approved for non-small cell lung cancer, metastatic HER2 negative breast cancer, metastatic renal cell carcinoma, and second line treatment of glioblastoma.[5]

Despite these promising clinical results, the effectiveness of BV is heavily dependent on the type of tumor, and different types of tumors have shown significantly different responses to VEGF blockade.[6] In addition to variability in effectiveness across tumor types, another difficulty that anti-angiogenic drugs face is that tumors can find a way around the VEGF pathway over time, and resume angiogenesis.[7] Furthermore, VEGF inhibitors can have significant toxicities, increasing the importance of targeting therapy to responders.[8] As a result of these difficulties in anti-angiogenic therapy, it is clear that the ability

*These authors contributed equally to this work.

†These authors contributed equally to this work.

Address all correspondence to: Andreas H. Hielscher, Columbia University, Department of Biomedical Engineering, 351 Engineering Terrace, 500 W. 120th Ave, New York, New York 10027. Tel: 212-854-5080; E-mail: ahh2004@columbia.edu.

0091-3286/2012/$25.00 © 2012 SPIE

to monitor the tumor progression and response to treatment in vivo will be valuable for improving effectiveness.

Current methods that have been explored for visualizing tumor angiogenesis and drug responsiveness include positron emission tomography (PET), magnetic resonance imaging (MRI), and ultrasound imaging (US). PET imaging uses radioactive tracers such as fluorodeoxyglucose (FDG), or ^{15}O, to look at tumor metabolism or perfusion.[9] MRI studies looking at angiogenesis typically focus on dynamic contrast enhanced MRI (DCE-MRI), which uses an injected paramagnetic contrast agent to generate maps of blood flow or permeability.[10] Ultrasound imaging of angiogenesis typically uses either power Doppler to assess the larger vessels, or injected microbubbles as a contrast agent to image blood flow in the smaller vessels [known as contrast enhanced ultrasound (CEUS)].[11] PET, DCE-MRI, and CEUS all require an injection of an exogenous contrast agent. Contrast agents can have adverse effects,[12] increase the time required for imaging protocols, and the injection of these agents introduces an additional variable that can be difficult to control in longitudinal studies.

DOT is a non-invasive imaging modality that uses light in the red to near-infrared range (650 to 900 nm) to probe tissue for physiologically relevant information. The light that passes through the tissue is absorbed and scattered by optically-relevant chromophores including oxy- and deoxy-hemoglobin, water, and fat. By detecting the transmitted and reflected light at various angles around the tissue, it is possible to reconstruct three-dimensional (3D) images of the distribution of the chromophores in the sample. This technology is currently undergoing clinical trials in a variety of settings, including breast cancer imaging,[13] the visualization of brain function,[14] and the diagnosis of arthritis.[15] Overall, the use of non-ionizing radiation, coupled with high sensitivity to oxygenated hemoglobin (HbO_2) and deoxygenated hemoglobin (Hb), short imaging times, and no need for exogenous contrast agents make this an attractive new imaging modality. Here we use 3D DOT images to visualize the hemoglobin concentration within tumors in small animals.

In this study, we used two tumor models with previously characterized and divergent responses to VEGF inhibition. Xenografts from the SK-NEP-1 human Ewing family tumor cell line[16] are highly responsive to various anti-VEGF agents, with significant loss of vasculature and inhibition of growth. In contrast, xenografts from the NGP human neuroblastoma cell line continue to grow with only slight restriction and minimally destabilized vessels.[17–20] Using DOT, we asked if differences in perfusion-related parameters could differentiate between the responder (SK-NEP-1) and non-responder (NGP) tumor models, and whether such changes could be detected within days of the start of treatment with the anti-VEGF antibody BV. We found that DOT image can distinguish responders from non-responders as early as one day after treatment, and confirmed these findings with MRI T2 relaxometry and lectin perfusion imaging. Our findings suggest that a DOT image can provide a rapid readout of tumor responsiveness to VEGF inhibition.

2 Methods

2.1 *Tumor Preparation*

Approximately one million NGP or SK-NEP-1 cells were injected intrarenally into four- to six-week-old NCR female nude mice (Taconic, Germantown, NY), as previously described,[17,18] and the resulting xenografts were monitored for growth using bioluminescence. At a threshold corresponding to 1 to 2 g, tumors were randomized to control or treatment groups (cohort size: five to six mice per treatment group). DOT and MRI imaging of the tumors was performed at Days 0, 1, 3, and 5. An injection of 0.2 mL of BV (2.5 mg/mL) was administered intravenously via the tail vein following the imaging sessions on Days 0 and 3. Albumin was used as a placebo for control studies (Con). Animals were euthanized by CO_2 inhalation at Day 5 after serial imaging studies (DOT and MRI), and at Days 0, 1, 3, and 5 for lectin perfusion analysis. All animal experiments were approved by the Columbia University Institutional Animal Care and Use Committee.

2.2 *Diffuse Optical Tomography (DOT)*

DOT imaging was performed with a continuous-wave optical tomography system developed in our laboratory (Columbia University, NY).[21] The system uses 16 sources to illuminate the target with two wavelengths (765 and 830 nm), and has 32 fibers to detect the scattered and transmitted light through the target. The optical fibers surround a cylinder made of white Delrin material with a wall thickness of 1.7 mm, a diameter of 3.2 cm and a height of 10 cm. The fibers are arranged in two rings separated by 1.25 cm, and with an alternating pattern of source-detector-detector-source. The animals were suspended vertically in the cylinder and held in place by a nose code that was also used to administer anesthesia (isofluorane gas 1 to 2%). For each imaging time point, the spine of the mouse was aligned with the same source fiber and the ears were carefully positioned to maintain precise vertical alignment. Intralipid® 1% (diluted from Intralipid® 20%, Baxter Healthcare Corp.) was used as a matching liquid surrounding the mouse to prevent edge artifacts. The Intralipid® 1% was warmed to 37 °C in order to maintain a stable mouse body temperature. Either prior to or following the mouse imaging a reference measurement was also acquired using Intralipid® 1%.

Data was acquired at 6.9 Hz with a dynamic range of ~190 dB.[21] Three hundred frames (~45 seconds of data) were collected at Days 0, 1, 3, and 5, along with a homogeneous reference image of Intralipid® 1%. The 300 frames were averaged to compute the mean and standard deviation data for each source-detector pair and then normalized to the homogenous reference prior to reconstruction into 3D images of oxygenated hemoglobin concentration ($[HbO_2]$), deoxygenated hemoglobin concentration ([Hb]), and total hemoglobin concentration ([THb]). We assumed that changes in absorption (i.e., $[HbO_2]$, [Hb], [THb]) would most strongly reflect tumor responsiveness to BV and, thus, did not include scattering parameters in our reconstruction. All image reconstructions were performed using a recently developed PDE-constrained multispectral imaging method[22] that employs the equation of radiative transfer as a light propagation model. The 3D volume mesh used in these reconstructions involved approximately 16,000 tetrahedral elements and the total reconstruction time for one image was approximately 2 hours on a Dual Core Intel Xeon 3.33 GHz processor.

2.3 *MRI T2 Relaxometry*

MRI is routinely used for high-resolution anatomical and physiological imaging in numerous clinical applications, including determination of tumor size, location, and perfusion.[23] MRI studies that visualize hemodynamic parameters typically employ gadolinium-based contrast agents.[24] To circumvent the potential

complications due to contrast agents, we adapted an approach first introduced by Teicher et al.[25] that uses T2 relaxometry to derive information about blood volume without the use of contrast agents. We applied this approach to determine relative blood volume fractions in tumors.

A vertical 9.4 T microimaging system (DRX400, Bruker-Biospin, Billerica, MA, USA) was used to perform abdominal MR imaging. The mice were anesthetized using isoflurane gas (1 to 2%) and their respiration was monitored and gated during the experiment. All experiments were carried out with a single-element 30-mm-diameter birdcage RF coil.T2-weighted images were acquired using 2D axial and coronal rapid acquisition with relaxation enhancement (RARE) pulse sequences. Imaging parameters included a pulse echo time of TE = 50 ms, a repetition time (TR) varying from 2700 to 3900 ms, an echo train of 8, a matrix size of 128×128, a slice thickness of 1 mm, an inter-slice gap of 0.2 mm, and a field of view (FOV) varying from 2.5 to 3 cm.

The T2 images were used to calculate the relative blood volume fraction in the tumors. Previous studies,[26–28] report a linear relationship between the changes in the transverse relaxation rate ($\Delta R2$) and the changes in deoxy-hemoglobin concentration (Δ[Hb]), a marker for blood volume. The relationship between $R2$ and [Hb] is linear:

$$R2 = R0 + k_2[\mathrm{Hb}] \Rightarrow \Delta R2 = \Delta R0 + k_2 \Delta[\mathrm{Hb}], \quad (1)$$

where $\Delta R0$ is the relaxometry contribution of $\Delta R2$ that is not the result of [Hb] changes, and k_2 is a tissue-specific constant. If we assume that the relaxation rate changes are caused by changes in the deoxy-hemoglobin concentration only, then $\Delta R0$ is zero. To reduce physiological variations that could affect $R0$, we maintained standard scan times and respiratory rates among all mice.

In a spin-echo sequence, the transverse relaxation rate change is related to the signal intensity using the logarithmic expression:

$$\Delta R2 = \ln(S_{\mathrm{pre}}/S_{\mathrm{post}})/\mathrm{TE}., \quad (2)$$

where TE is the effective echo time and S_{pre}, S_{post} are the signal intensities of the region of interest (ROI) in the corresponding T2 images before and after treatment respectively. T2 images were preferred to T1 for the blood volume measurements because they provided significantly improved anatomical information.[29] T2 images were also preferred to T2* images due to their superior performance in depicting heterogeneous distributions of small-field disturbances (derived from arterioles, capillaries, and venules), as opposed to large vessels.[26]

The coronal T2 view allowed the selection of a larger ROI within the tumors, since the tumors appeared to expand more on the anteroposterior axis than on the lateral or dorsoventral axes across the five-day treatment period. However, axial T2 images were used for the $\Delta R2$ measurements in cases where the depiction of the tumor was not clear in the coronal view. The ROI signal intensities were normalized over the signal intensity of the urine (reference signal) on the unaffected kidney. In selecting the ROI, we chose a region with very homogeneous contrast and attempted to avoid large vessels within the tumor as well as necrotic and possibly hypoxic regions in the tumor core. The selected image plane, slice, and ROI dimensions remained as consistent as possible across the different days. The same operator processed all the images.

2.4 *Lectin Perfusion Studies*

At euthanasia, mice were injected with fluorescein-labeled Lycopersicon esculentum lectin (100 μg/100 μl PBS, Vector Laboratories, Burlingame, CA). Vasculature was fixed by infusing 1% paraformaldehyde. 40-μm sections were cut using a vibratome, and digital images subjected to computer-assisted quantitative analysis of tumor vessel architecture.[30,31] After binarization, microvessel density (MVD) was estimated by the total number of white pixels per field as determined by the method of Wild et al.[30] The total number of images analyzed ranged from 35 to 67 for SK-NEP-1, and from 51 to 74 for NGP.

2.5 *Statistical Methods*

To assess overall differences between the groups of mice, a linear mixed effects regression model was implemented using the SAS PROC MIXED procedure (SAS Software Version 9.1, SAS Institute, Cary, NC). The model estimates linear trajectories for each cohort over time, while accounting for comparisons among repeated measurements from the same mice. The intercept was treated as a random effect and covariate to account for the differences between mice at baseline. The maximum likelihood method was used to estimate the regression coefficients. DOT imaging employed a linear model for the [THb] at Days 0, 1, 3, and 5, using the slope of linear fit for comparison between cohorts. Since all MRI measurements correlated with Day 0, we employed a linear model for the relative signal change at Days 1, 3, and 5, using the intercept of the linear fit for comparison between cohorts. In this case, the intercept was more meaningful than the slope of the linear fit due to the lack of a Day 0 data point. Comparisons of DOT and MRI parameters between BV-treated and control tumors at Days 1, 3, and 5 were calculated using unpaired two-tailed Student's t-tests, with alpha set at 0.05. Lectin perfusion data was analyzed with one-way ANOVA and post-analysis with Tukey's multiple comparison test (GraphPad Prism 5.0 Software, San Diego, CA).

3 Results

3.1 *DOT*

Continuous-wave DOT [Fig. (1a)] was performed using near-infrared light to illuminate the target sequentially from multiple angles while measuring transmitted and reflected light intensities, allowing sensitive detection of changes in concentrations of chromophores (e.g. oxy, deoxy-hemoglobin, and total hemoglobin). Figure 1(d) shows 3D volume images of total hemoglobin [THb]. Overall, we observed a strong decrease in total hemoglobin [THb] at least once over the five-day experimental period in BV-treated SK-NEP-1 tumors. In Fig. 1(d), [THb] in the BV-treated SK-NEP-1 tumors reached a nadir at Day 3, then partially recovered at Day 5. In contrast, in control SK-NEP-1 tumors, and both control and BV-treated NGP tumors, [THb] steadily increased over the five-day period.

The observed effects are further illustrated through axial slices taken from the 3D reconstruction through the plane of peak [THb]. Figure 2(a) shows four mice from the BV-treated SK-NEP-1 cohort, and Fig. 2(b) shows four mice from the BV-treated NGP cohort. At some point over the five days all BV-treated SK-NEP-1 mice show a drop in [THb], while

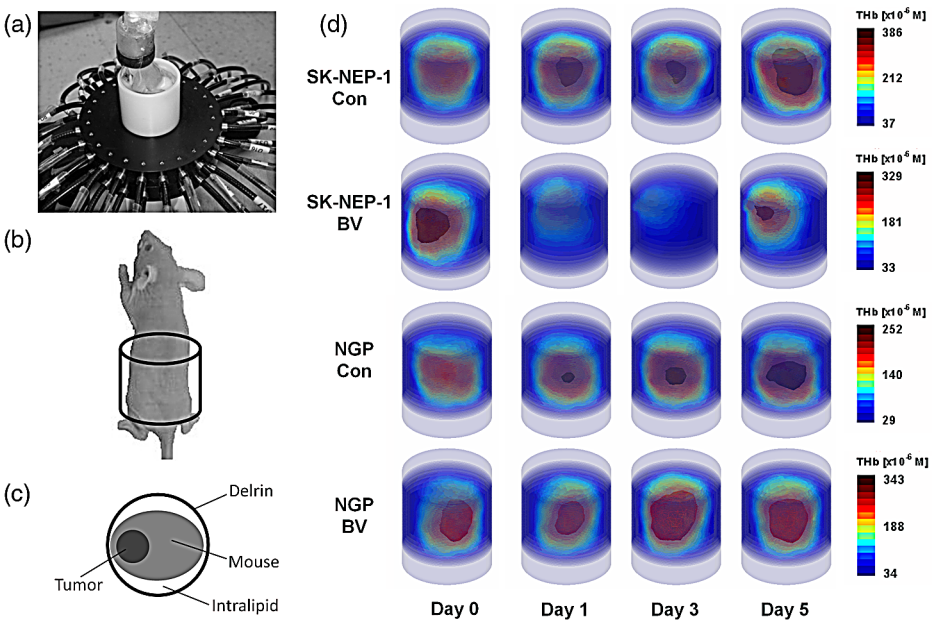

Fig. 1 (a) The experimental setup showing a mouse surrounded by Intralipid® in the imaging cylinder with the two rings of optical fibers surrounding the tumor region.[22] Also shown are diagrams outlining (b) the region of the mouse shown in the 3D volume images and (c) the orientation of the mouse and tumor in the 2D axial images, and (c) 3D [THb] images showing a 2×3 cm cylindrical volume encompassing the tumor-bearing portion of representative mice from the SK-NEP-1 Con ($n = 5$), SK-NEP-1 BV ($n = 5$), NGP Con ($n = 6$), and NGP BV ($n = 6$) cohorts at Days 0, 1, 3, 5. A steady increase in [THb] over the five days is noticeable in the SK-NEP-1 Con, NGP BV, and NGP Con cohorts. In contrast, the SK-NEP-1 BV cohort showed a strong decrease in [THb] at Days 1 and 3 followed by a rebound at Day 5.

NGP mice showed an increase in [THb] over the five days. It appears as though some BV-treated NGP mice do show mild signs of suppressed vascularization [Fig. 2(b), rows 3 and 4] due to the drug, although the effect is much lesser than in the SK-NEP-1 cohort.

To quantify these effects, a 5 mm^3 cube was selected centered on the highest-intensity voxel, and mean [THb] of the voxels within that cube calculated. Figure 3 shows the mean [THb] over the five days, with a linear fit generated by a mixed-effects model.[32] For SK-NEP-1 tumors, mean [THb] showed a divergent trend between BV-treated and control cohorts with a significant difference in the slope of the linear fit for each cohort ($P = 0.02$). In contrast, for NGP tumors, the mean [THb] increased in both BV-treated and control cohorts over the five days with no significant difference in the slope of the linear fit for each group ($P = 0.81$).

In Fig. 4, the percentage change in mean [THb] from Day 0 significantly distinguishes between SK-NEP-1BV-treated and control cohorts at Day 1 (BV: $-18 \pm 15\%$; Con: $19 \pm 27\%$; $P = 0.034$) and Day 5 (BV: $-9 \pm 22\%$; Con: $42 \pm 37\%$; $P = 0.034$). No such distinction was seen in NGP BV-treated and control cohorts, which showed an overall increase by Day 5 (BV: $5 \pm 14\%$; Con: $5 \pm 33\%$; $P = 0.99$). Oxy- and deoxy-hemoglobin concentrations, [HbO_2] and [Hb], followed

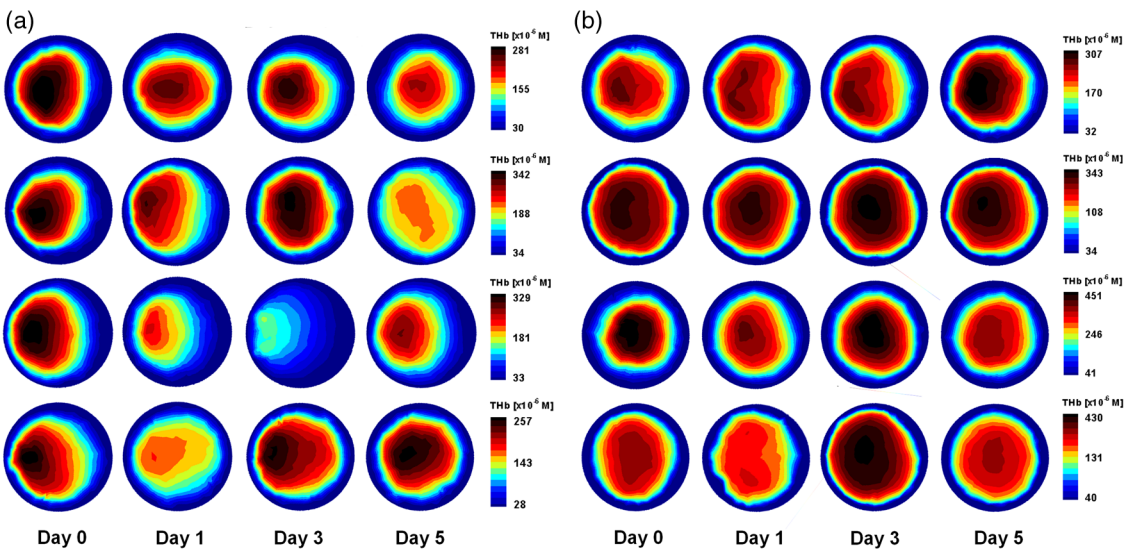

Fig. 2 2D axial slices through the plane of peak [THb] are shown for four animals from the (a) BV-treated SK-NEP-1 cohort and (b) BV-treated NGP cohort. The images are oriented with the tumor at 9 o'clock, as illustrated in Fig. 1c.

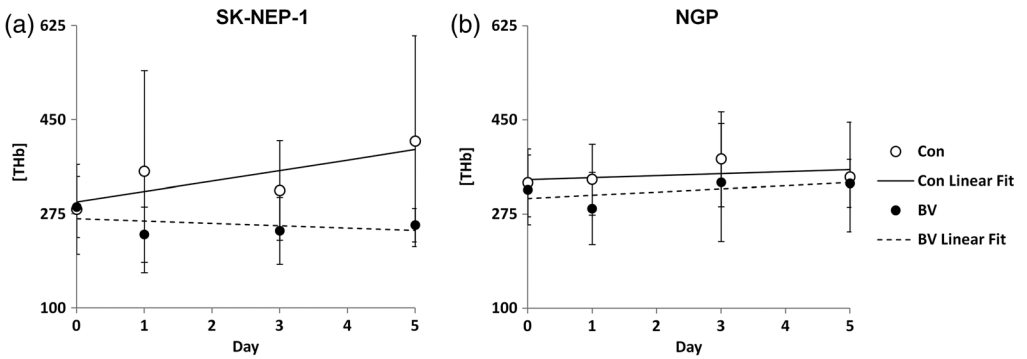

Fig. 3 [THb] was quantified in the tumor region by selecting a 5 mm^3 cube surrounding the peak voxel. The slope of the linear fit is significantly different between the SK-NEP-1 BV-treated (BV) and control (Con) cohorts ($P = 0.02$). No much significance is seen between the NGP BV-treated and control cohorts ($P = 0.81$).

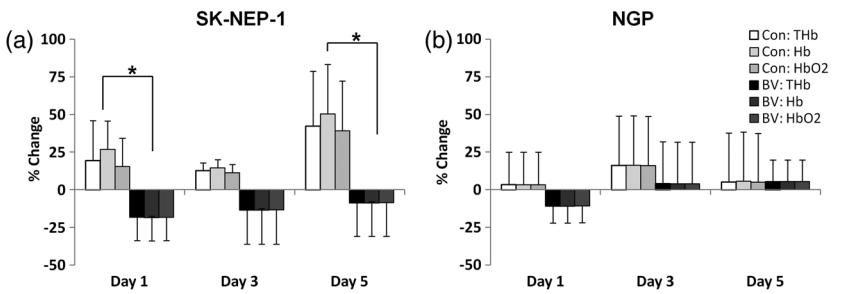

Fig. 4 Mean and standard deviations of total-, oxy- and deoxy-hemoglobin concentrations, [THb], [Hbo_2] and [Hb], over the five days. [Hbo_2] and [Hb] followed similar trends to [THb], with BV causing a decrease in (a) SK-NEP-1 but not in (b) NGP tumors (*$P < 0.05$).

similar trends to [THb], with BV causing a decrease in [HbO_2] and [Hb] in SK-NEP-1 but not in NGP [Figs. 4(a) and 4(b)]. This finding suggests that a blood volume reduction is the leading cause for this observation, rather than a change in blood oxygen saturation.

3.2 *MRI T2 Relaxometry*

MRI T2 relaxometry has previously been used to derive steady-state blood flow measures in the brain.[25] We have adapted this technique to determine relative blood volume in tumors, by using the T2 images to determine the transverse relaxation rate ($\Delta R2$). Since the change in the transverse relaxation rate ($\Delta R2$) is linearly related to the change in the deoxygenated hemoglobin concentration Δ[Hb],[26–28] $\Delta R2$ can be used to determine relative blood volume. Figure 5 shows axial examples of T2-weighted MR images taken just before the injection of BV (Day 0), and 1, 3, and 5 Days after the injection. In the BV-treated SK-NEP-1 tumors there is a visible increase in the T2 signal intensity (brightness). This indicates that $\Delta R2$ and, thus, the relative blood volume, decreases with BV treatment. In comparison, the T2 signal intensity in control SK-NEP-1 tumors and both control and BV-treated NGP tumors remained relatively constant or decreased, indicating that the relative blood volume remained constant or increased, respectively.

Quantifying the transverse relaxation rate ($\Delta R2$), we found that BV caused a rapid (after one day) decrease in the relative blood volume in SK-NEP-1 tumors as determined by a significant decrease of $3.47 \pm 2.77\ s^{-1}$ ($P = 0.021$) in the $\Delta R2$ [Fig. (6)]. By Day 3 and Day 5, the effect of BV on the relative blood volume persisted but lessened (reduction of $0.91 \pm 2.22\ s^{-1}$ and $1.1 \pm 1.95\ s^{-1}$, respectively). SK-NEP-1 control tumors exhibited no statistically significant changes in the $\Delta R2$. BV-treated and control NGP tumors exhibited either stable or increased $\Delta R2$ over time. To statistically evaluate the overall response over the entire five days of the study, we employed a linear mixed-effects model.[32] A linear fit to Days

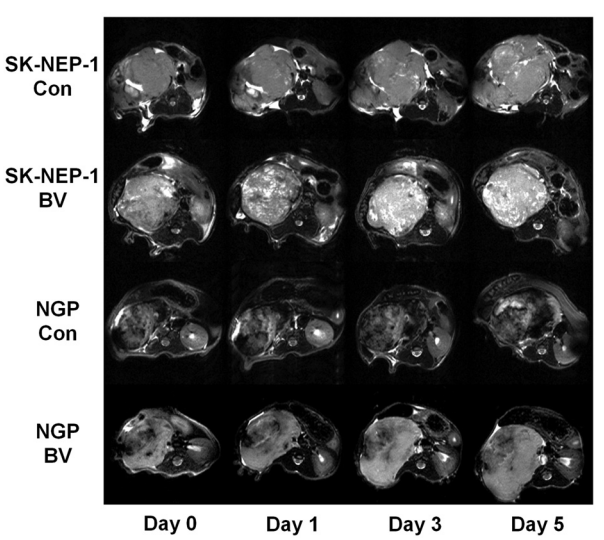

Fig. 5 T2 spin-echo axial MR images of SK-NEP-1 and NGP renal tumors in NCR Nude mice. The axial slices were obtained at Days 0, 1, 3, and 5 after an initial injection with either bevacizumab (BV) or albumin control (Con) at Day 0. All animals received a second injection on Day 3 prior to imaging. 2D images are shown for representative mice from the SK-NEP-1 Con ($n = 5$), SK-NEP-1 BV ($n = 5$), NGP Con ($n = 6$), and NGP BV ($n = 5$) cohorts.

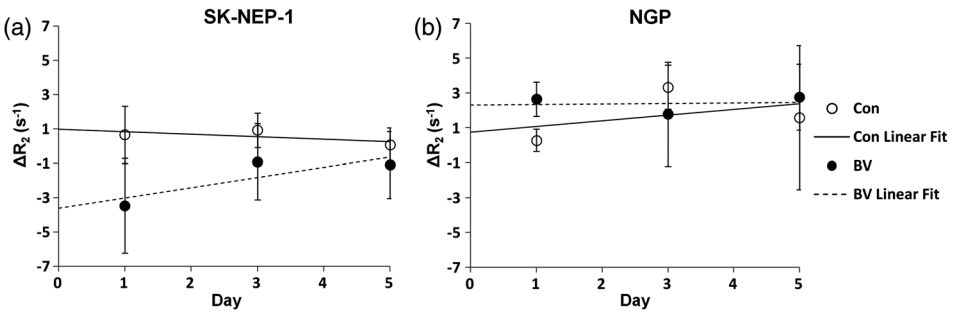

Fig. 6 Changes in the transverse relaxation rate ($\Delta R2$) were quantified in a specific region of interest (ROI) with homogeneous tissue contrast within the tumor. The same region was selected throughout the tumor images over the five days. A mixed effects model was used to estimate the linear trajectories for each cohort. The slope of the linear fit is significantly different between the SK-NEP-1 BV-treated and control cohorts ($P = 0.0014$). No such significance is seen between the NGP BV-treated and control cohorts ($P = 0.1037$).

1, 3, and 5 demonstrated a significant difference between the intercept of the SK-NEP-1BV-treated cohort and the control cohort ($P = 0.0014$), but no such difference between the NGP BV-treated cohort and the control cohort ($P = 0.1037$).

In addition to the transverse relaxation rate, we quantified the tumor mass from MR images. This was performed by manually outlining the left kidney in the axial T2 images and generating 3D reconstructed views of the tumors. The mass value was estimated from the product of the total number of voxels within the boundary of each tumor and the voxel resolution, also taking into consideration the interslice gap of the 2D MR images. Treatment of SK-NEP-1 mice with BV essentially arrested tumor growth over the five-day period, compared with continued growth in the control tumors [Fig. (7)]. Growth of NGP tumors was unaffected by BV treatment. These results along with the analysis of lectin perfusion studies of the vasculature, shown in Sec. 3.3, verify our DOT classification of SK-NEP-1 as a responder and NGP as a non-responder to VEGF blockade therapy.

3.3 *Lectin Perfusion*

Established SK-NEP-1 and NGP tumors were injected IV with fluorescein-labeled L. esculentum lectin, prior to sacrifice at Day 0, or after 1, 3, or 5 days of treatment with either the control

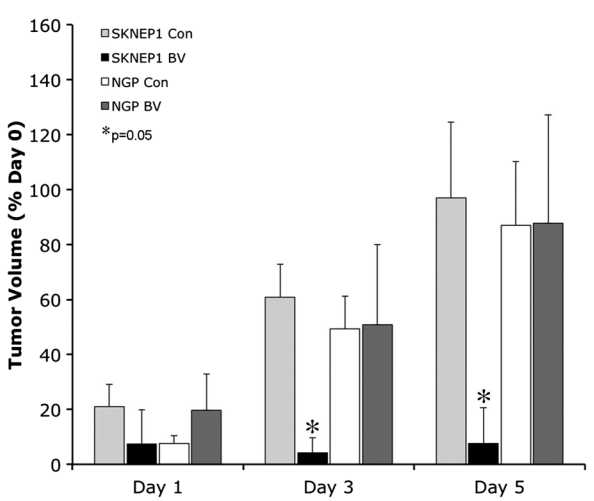

Fig. 7 The temporal progression of the percentage mass volume-changes of the tumors as computed by 3D reconstructed T2 MRI views of the tumors. The percentage mass volume changes from Day 0 to Day 5 were recorded for all mice. BV treatment significantly inhibited tumor growth in SK-NEP-1 xenografts at Days 3 and 5 in comparison to control, but not in NGP xenografts ($^*P < 0.05$).

vehicle or BV [Fig. (8a)]. There is a noticeable decrease in the tumor vascularization in the SK-NEP-1 BV-treated tumors by Day 1, which persists at Day 3 and Day 5. This decrease in vascularization is not evident in NGP BV-treated tumors.

Quantified changes in lectin perfusion studies of tumor vasculature were consistent with changes detected by DOT and MRI T2 relaxometry [Fig. (8b)]. As compared to Day 0 controls, MVD in BV-treated SK-NEP-1 tumors decreased by 65% at Day 1, 74% at Day 3, and 77% at Day 5 ($P < 0.001$, each) and differed significantly from control SK-NEP-1 tumors at Days 1, 3, and 5 ($P < 0.001$, each). MVD decreased by 51% in BV-treated NGP tumors at Day 3 ($P < 0.01$) followed by a rebound back to baseline levels at Day 5. There was no significant difference between control and BV-treated NGP tumors at any day.

4 Discussion

Biologically targeted agents hold promise for increasing effectiveness of cancer treatment, yet optimizing their use may require the development of new assessment strategies. In this set of preclinical studies, we demonstrated that it is possible to clearly distinguish responder from non-responder tumors within five days of BV treatment [Fig. (3)]. Changes in total hemoglobin identified by DOT imaging at early time points correlates to changes in microvessel density (as observed by lectin perfusion imaging) and relative blood volume (as observed by MRI T2 relaxometry). The DOT images show a significant decrease in total hemoglobin in the tumor region over the five days, but no significant change in the blood oxygen saturation [Fig. (4)], leading us to believe that a blood volume reduction is the leading cause for this observation. This is confirmed by the change in relative blood volume observed in BV-treated SK-NEP-1 by the MRI T2 relaxometry studies [Fig. (6)].

These results underscore the importance of visualizing the tumor vascularity non-invasively for longitudinal studies. In both the DOT [Fig. (3)] and MRI [Fig. (6)] quantification of tumor [THb] and blood volume there are signs of rebounding effects in the BV-treated SK-NEP-1 and NGP tumors. This transitive response can be measured *in vivo*, using DOT, and provides valuable insight into the temporal dynamics of the vasculature in response to anti-angiogenic therapy. Further work is necessary to correlate how these observed transitive responses relate to changes in the vascular structure, namely normalization of vessel architecture.[33,34] In addition, the incorporation of other optical imaging techniques such as diffuse correlation spectroscopy (DCS)[35] and contrast-enhanced optical techniques[36]

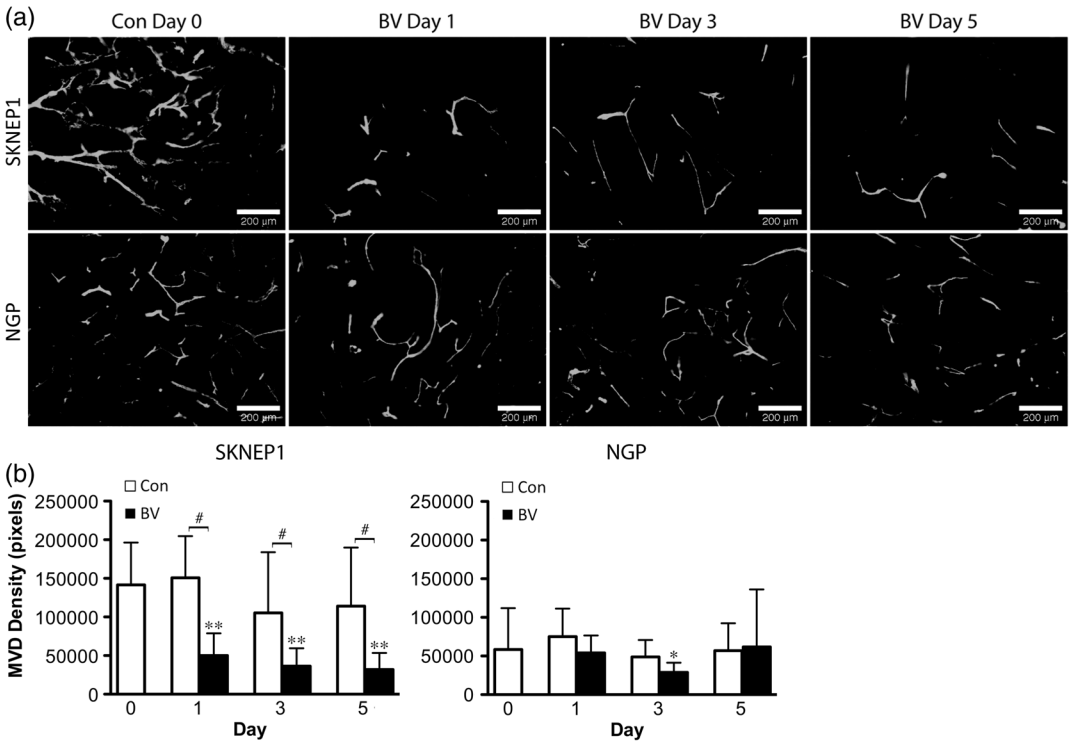

Fig. 8 Representative fluorescent images are shown in (a) for BV-treated SK-NEP-1 and NGP tumors at Days 0, 1, 3, and 5. A noticeable decline in vasculature is observed by Day 1 in SK-NEP-1 BV-treated mice, but not in NGP BV-treated mice. There is a significant drop in microvessel density (MVD) and (b) in SK-NEP-1 BV-treated tumors at Days 1, 3, and 5 ($^{**}P < 0.001$) compared with Day 0 control tumors, and with a significant difference in MVD between Con and BV-treated tumors at Days 1, 3, and 5 ($P < 0.001$). NGP BV-treated mice show a drop at Day 3 ($^{*}P < 0.001$), with a rebound at Day 5, and no significant differences between Con and BV-treated tumors on any day.

may enhance this work by further quantifying the changes in tumor perfusion and oxygenation due to BV treatment. More sophisticated image classification algorithms may also provide alternative ways of quantifying tumor response and could extend this work to use multiple image parameters to discriminate responders from non-responders, similar to work that has been performed using optical images for classification in rheumatoid arthritis[15] and breast cancer.[37]

DOT's advantages lie in its low-cost, short imaging times, and use of non-invasive and non-ionizing radiation. In addition, with no need for exogenous contrast agents, DOT is well suited to longitudinal studies that require repeated imaging. Our findings open the door for a number of non-invasive, longitudinal, pre-clinical studies, to improve our understanding of the subtleties of anti-angiogenic agents in an effort to increase the efficacy of these drugs. Furthermore, this study provides pre-clinical background as the field of DOT looks to translate these findings into therapy monitoring in the clinic.[13]

Overall, our study suggests that development of rapid, imaging-based assessments for human patients is feasible. Coordinated clinical use of DOT data can provide significant benefits for patients by enabling earlier and more effective clinical decision-making. For individuals with nonresponsive tumors, alternate regimens could be considered without waiting for overt therapeutic failure to occur, avoiding needless toxicity. Alternatively, those patients whose tumors demonstrated responsiveness could remain on treatment. Lastly, given the high cost of biologically-targeted therapies like BV, such early assessment of drug effectiveness may reduce the economic strains of cancer treatment for patients and families.

Acknowledgments

This work was supported in part by several grants from the National Institutes of Health: NCI-5R01CA124644 (to D.J.Y.); NCI-R21CA139173 (to M.A.B. and J.J.K.), and NCI-5R33CA118666 and NCI-5U54CA126513-039001 (to A.H.H.). In addition, J.J.K. was supported by grants from the Pediatric Cancer Foundation and the Sorkin Fund, D.J.Y. was supported by the Tay-Bandz Foundation, M.L.F. was partially supported by the Natural Sciences and Engineering Research Council of Canada (NSERC).

References

1. J. Folkman, "Tumor angiogenesis: therapeutic implications," *N. Engl. J. Med.* **285**(21), 1182–1186 (1971).
2. J. G. Bender et al., "Vascular remodeling and clinical resistance to anti-angiogenic cancer therapy," *Drug Resist. Updates* **7**(4–5), 289–300 (2004).
3. F. Kabbinavar et al., "Phase II, randomized trial comparing bevacizumab plus fluorouracil (FU) leucovorin (LV) with FU/LV alone in patients with metastatic colorectal cancer," *J. Clin. Oncol.* **21**(1), 60–65 (2003).
4. H. Hurwitz et al., "Bevacizumab plus irinotecan, fluorouracil, and leucovorin for metastatic colorectal cancer," *N. Engl. J. Med.* **350**(23), 2335–2342 (2004).
5. R. Pazdur, "FDA approval for bevacizumab," (2009), http://www.cancer.gov/cancertopics/druginfo/fda-bevacizumab.
6. K. J. Kim et al., "Inhibition of vascular endothelial growth factor-induced angiogenesis suppresses tumor growth in vivo," *Nature* **362**(6423), 841–844 (1993).
7. G. Bergers and D. Hanahan, "Modes of resistance to anti-angiogenic therapy," *Nat. Rev. Cancer.* **8**(8), 592–603 (2008).

8. K. Mulder et al., "The role of bevacizumab in colorectal cancer: understanding its benefits and limitations," *Expert Opin. Biol. Ther.* **11**(3), 405–413 (2011).
9. G. Niu and X. Chen, "PET imaging of angiogenesis," *PET Clin.* **4**(1), 11 (2010).
10. S. Zwick et al., "Assessment of vascular remodeling under antiangiogenic therapy using DCE-MRI and vessel size imaging," *J. Magn. Reson. Imag.* **29**(5), 1125–1133 (2009).
11. M. Lamuraglia et al., "Clinical relevance of contrast-enhanced ultrasound in monitoring anti-angiogenic therapy of cancer: Current status and perspectives," *Crit. Rev. Oncol. Hematol.* **73**(3), 202–212 (2010).
12. J. G. Penfield, "Nephrogenic systemic fibrosis and the use of gadolinium-based contrast agents," *Pediatr. Nephrol.* **23**(12), 2121–2129 (2008).
13. B. J. Tromberg et al., "Assessing the future of diffuse optical imaging technologies for breast cancer management," *Med. Phys.* **35**(6), 2443–2451 (2008).
14. A. Custo et al., "Anatomical atlas-guided diffuse optical tomography of brain activation," *Neuroimage.* **49**(1), 561–567 (2010).
15. A. H. Hielscher et al., "Frequency-domain optical tomography imaging of arthritic finger joints," *IEEE Trans. Med. Imag.* **30**(10), 1725–1736 (2011).
16. M. A. Smith et al., "SK-NEP-1 and Rhl are Ewing family tumor lines," *Pediatr. Blood. Canc.* **50**(3), 703–706 (2008).
17. J. Z. Huang et al., "Regression of established tumors and metastases by potent vascular endothelial growth factor blockade," *Proc. Natl. Acad. Sci. U.S.A* **100**(13), 7785–7790 (2003).
18. E. S. Kim et al., "Potent VEGF blockade causes regression of coopted vessels in a model of neuroblastoma," *Proc. Natl. Acad. Sci. U.S.A* **99**(17), 11399–11404 (2002).
19. D. H. Rowe et al., "Anti-VEGF antibody suppresses primary tumor growth and metastasis in an experimental model of Wilms' tumor," *J. Pediatr. Surg.* **35**(1), 30–32 (2000).
20. D. H. Rowe et al., "Suppression of primary tumor growth in a mouse model of human neuroblastoma," *J. Pediatr. Surg.* **35**(6), 977–981 (2000).
21. J. M. Lasker et al., "Digital-signal-processor-based dynamic imaging system for optical tomography," *Rev. Sci. Instrum.* **78**(8), 08706 (2007).
22. H. K. Kim et al., "PDE-constrained multispectral imaging of tissue chromophores with the equation of radiative transfer," *Biomed. Opt. Express.* **1**(3), 12 (2010).
23. R. R. Edelman et al., *Clinical Magnetic Resonance Imaging*, Elsevier, Philadelphia, PA (2005).
24. K. M. Johnson et al., "Gadolinium-bearing red cells as blood pool MRI contrast agents," *Magn. Reson. Mater. Med.* **40**(1), 133–142 (1998).
25. M. H. Teicher et al., "Functional deficits in basal ganglia of children with attention-deficit/hyperactivity disorder shown with functional magnetic resonance imaging relaxometry," *Nat. Med.* **6**(4), 470–473 (2000).
26. S. Remmele et al., "Concurrent MR blood volume and vessel size estimation in tumors by Robust and simultaneous $\Delta R2$ and $\Delta R2^*$ quantification," *Magn. Reson. Mater. Med.* **66**(1), 144–153 (2011).
27. G. Gambarota et al., "Characterisation of tumour vasculature in mouse brain by USPIO contrast-enhanced MRI," *Br. J. Canc.* **98** (11), 1784–1789 (2008).
28. C. M. Anderson et al., "Brain T2 relaxation times correlate with regional cerebral blood volume," *Magn. Reson. Mater. Phys., Biol. Med.* **18**(1), 3–6 (2005).
29. H. Moreno et al., "Longitudinal mapping of mouse cerebral blood volume with MRI," *NMR Biomed.* **19**(5), 535–543 (2006).
30. R. Wild et al., "Quantitative assessment of angiogenesis and tumor vessel architecture by computer-assisted digital image analysis: effects of VEGF-toxin conjugate on tumor microvessel density," *Microvasc. Res.* **59**(3), 368–376 (2000).
31. J. Huang et al., "TNP-470 promotes initial vascular sprouting in xenograft tumors," *Mol. Canc. Therapeut.* **3**(3), 335–343 (2004).
32. N. M. Laird and J. H. Ware, "Random-effects models for longitudinal data," *Biometrics.* **38**(4), 963–974 (1982).
33. R. K. Jain, "Normalization of tumor vasculature: An emerging concept in antiangiogenic therapy," *Science* **307**(5706), 58–62 (2005).
34. M. M. Darpolor, R. C. Molthen, and K. M. Schmainda, "Multimodality Imaging of abnormal vascular perfusion and morphology in Preclinical 9L Gliosarcoma Model," *PloS One.* **6**(1) (2011).
35. R. C. Mesquita et al., "Direct measurement of tissue blood flow and metabolism with diffuse optics," *Philos. Transact. A Math. Phys. Eng. Sci.* **369**(1955), 4390–4406 (2011).
36. M. Eisenblatter et al., "Optical techniques for the molecular imaging of angiogenesis," *Eur. J. Nucl. Med. Mol. Imag.* **37**, S127–S137 (2010).
37. D. R. Busch et al., "Computer aided automatic detection of malignant lesions in diffuse optical mammography," *Med. Phys.* **37**(4), 1840–1849 (2010).